“ETFA” Bearings Strengthened by Fine Microstructure Design

Masahiro YAMADA*
Chikara OHKI*
Naota YAMAMOTO**

NTN designed a special heat treatment to improve bearing properties by resulting in a fine microstructure of steel. The resulting fine microstructure consists of homogeneous martensite blocks and precipitations of a refined size. Testing shows specimens with fine microstructure had high impact strength and wear resistance. Fine microstructure test bearings also showed superior rolling contact fatigue lives under both clean and contaminated lubrication conditions. **NTN** calls these bearings “ETFA”. In this paper, we explain the details of ETFA bearings.

1. Introduction

With a shift toward lower fuel consumption of automobiles and increasing compactness of industrial machinery, there is a trend toward increasingly severe bearing operating conditions. Typically these include higher contact surface pressure and lower viscosity of lubricating oils. These increasingly harsh use environments may promote problems such as flaking that originates from an indentation and shorten bearing life. Therefore, there is a need for higher bearing strength.

To achieve higher bearing strength, it is crucial to strengthen the steel material. There are a number of methods for strengthening steel and one of these involves refinement of crystal grains[1]. This can be regarded as a strengthening method that hinders dislocation motion due to the increase in grain boundaries and changes the plastic properties of steel. There has previously been discussion of the effects of the size of prior austenite grains (referred to hereafter as “prior γ grains”) on strengthening by the refinement of crystal grains in quenched steel. However, there are few examples of comparative examination of the size of martensite grains actually formed due to quenching[2]. In recent years, it has been thought that the size of martensite blocks (referred to hereafter as “blocks”) that are the effective crystal grains is the dominant factor in determining the strength of steel. Therefore, to strengthen steel through crystal grain refinement, it is necessary to produce a more refined martensite structure rather than refining the prior γ grains[3)-6)].

The authors have already developed long-life, high-strength bearings made of JIS SUJ2 in which blocks were refined through special heat treatment[7]. These through hardened bearings had blocks strengthened through refinement, and were enhanced with improved anti-wear performance through nitriding[7)-9)].

Recently, we have used the aforementioned heat treatment technology to develop new bearings made of low-carbon steel with refined blocks for longer life and higher strength. **NTN** calls these newly developed bearings “ETFA,” and we are currently moving toward practical application.

This article describes the details of these ETFA bearings.

2. Fine microstructure of ETFA

2.1 Material and state of precipitation formation

The material used is low-carbon steel containing Cr and Mo. The fine microstructure of low-carbon steel is controlled by applying carbonitriding treatment and grain refinement treatment. **Table 1** shows a comparison of ETFA characteristics with the characteristics of conventional carbonitriding treated bearings (referred to hereafter as the “conventional product”)[10]. Compared to the conventional product, the prior γ grains, blocks, and precipitations of ETFA are finer than the conventional product, and the number density of precipitations is high.

Fig. 1 shows a typical example of the depth distributions of carbon and nitrogen concentrations in ETFA measured with an Electron Probe Micro Analyzer (EPMA). Multiple sharp rises in concentration attributable to precipitations were confirmed in the surface layer. It is evident that carbides, nitrides, and carbonitrides are present at high density and with high refinement.

Fig. 2 shows a scanning electron microscope (SEM) image of prior γ grain boundaries and precipitations in the raceway surface layer. The crystal grains of ETFA are fine and precipitations are homogeneously dispersed.

* Advanced Technology R&D Center
** Application Engineering Dept., Industrial Business Headquarters

Table 1 Feature of the developed bearings

Item	Conventional product	ETFA
Heat treatment	Carbonitriding quenching	Carbonitriding quenching Grain refinement treatment
Carbon concentration	Standard	Standard
Nitrogen concentration	Standard	Standard
Residual γ amount	Standard	Standard
Size of precipitations	Standard	Fine
Number of precipitations	Standard	Numerous
Size of prior γ grain	Standard	Fine
Size of martensite blocks	Standard	Fine
Hardness	Standard	Standard

2.2 Condition of block formation

Fig. 3 shows images of prior γ grains and blocks in the raceway surface layer. The block images are inverse pole figure crystal orientation maps measured using the electron backscatter diffraction (EBSD) method. The prior γ grains and blocks of ETFA are fine compared to the conventional product. **Fig. 4** shows the {011} pole figure for blocks. The block crystal orientation density is lower overall than that of conventional products and crystalline orientation is low.

Fig. 5 shows the average grain size of these blocks and their average aspect ratio. These values were calculated for blocks corresponding to a specific area ratio. That is, blocks within the field of observation are added together in order of their area, and this is the average value for those grains when their total area corresponds to 30, 50, or 70 % of the block total area. The difference in block diameter compared to the conventional product increases as the area ratio decreases, and a similar trend is event for the aspect ratio as well.

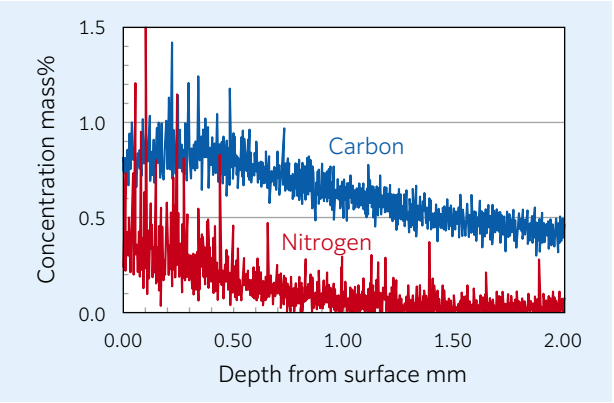

Fig. 1 Typical depth profiles of C and N concentrations of the developed bearings

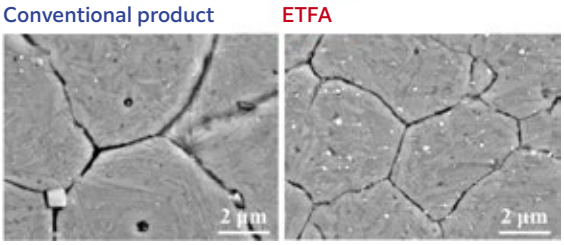

Fig. 2 SEM-micrographs of prior austenite grain boundary and precipitations near race surfaces of the bearings

As indicated above, the formation of precipitations and blocks is refined and homogeneous on the raceway surfaces of ETFA bearings.

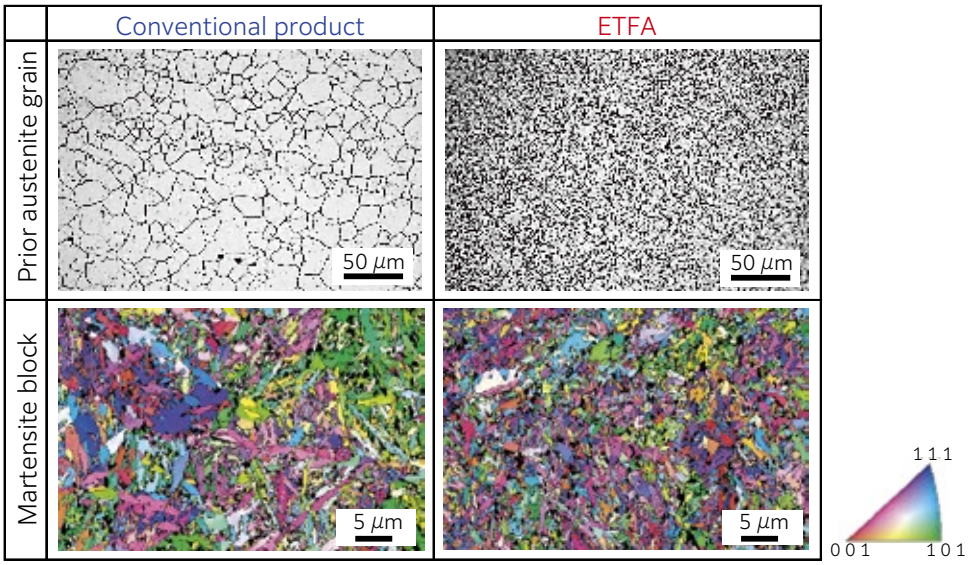

Fig. 3 Observation images of prior austenite grain and martensite block near race surfaces of the bearings

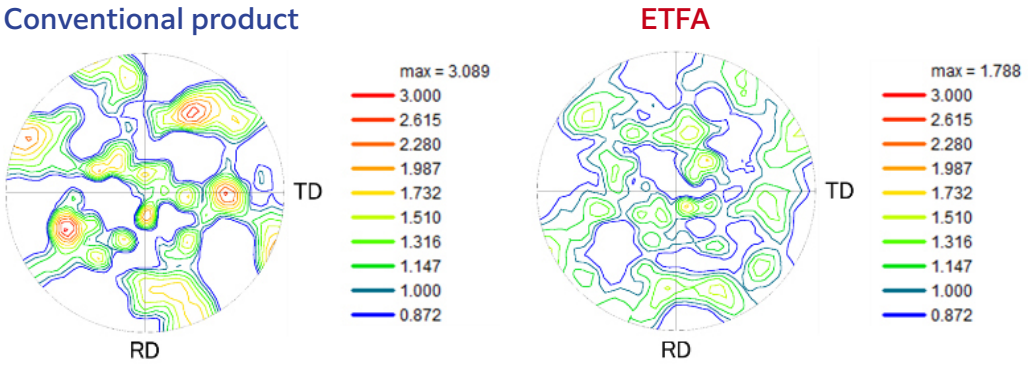

Fig. 4 {011} pole figure of martensite block near race surfaces of the bearings

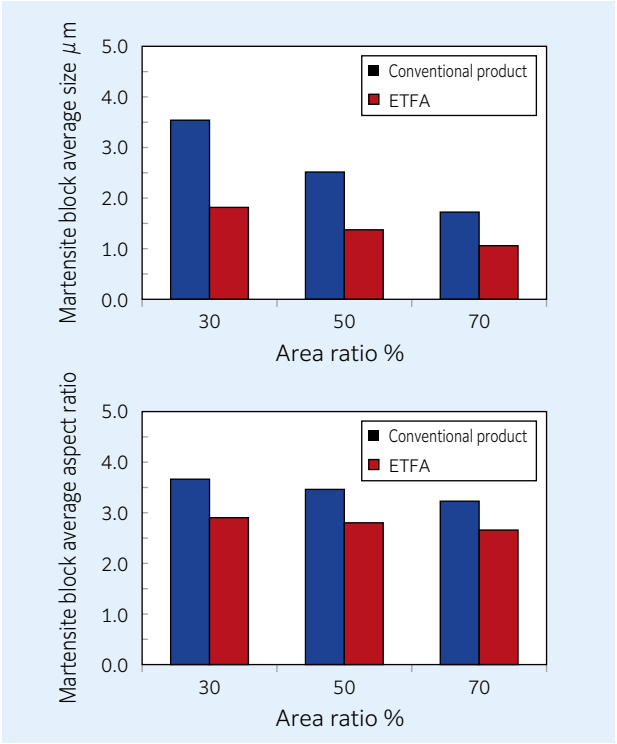

Fig. 5 Martensite block size and aspect ratio near race surfaces of the bearings

3. Rolling fatigue life of ETFA bearings

3.1 Rolling fatigue life test conditions

Rolling fatigue life testing was carried out under both clean and contaminated lubrication conditions. **Fig. 6** shows a schematic drawing of the test rig, and **Table 2** shows the test conditions[7]. The test bearing used in the life test was a tapered roller bearing. The life test with clean lubrication was carried out with N=5 for bearing A (inner diameter 30 mm × outer diameter 62 mm × width 17.25 mm). To improve the reliability of evaluation results in the life test with contaminated lubrication, testing was carried out with N=6–9 for bearings A and B in two sizes (inner diameter 85 mm × outer diameter 165 mm × width 56–58 mm). To increase contact surface pressure of the raceway in testing of bearing B, the number of rolling elements was reduced from the standard 17 to 5.

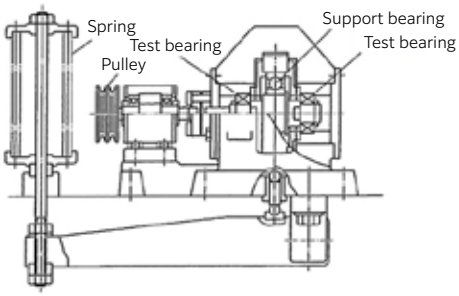

Fig. 6 Schematic drawing of the life test rig

Table 2 Conditions of the life test

Item	Bearing A	Bearing B
Basic dynamic radial load rating	48.5 kN	Conventional product: 150 kN ETFA: 168 kN (Number of rolling elements: 5)
Radial load	17.64 kN	53.9 kN
Axial load	1.47 kN	29.4 kN
Max. contact surface pressure	2.5 GPa	Conventional product: 2.9 GPa ETFA: 2.8 GPa
Inner ring rotational speed	2,000 min^{-1}	500 min^{-1}
Lubricating oil viscosity	ISO VG 56	ISO VG 100
Contaminant type	High speed tool steel dust	High speed tool steel dust
Contaminant size	100 - 180 μm	100 - 180 μm
Contaminant hardness	700 - 800 HV	700 - 800 HV
Amount of contaminant in lubricating oil	1.0 g/L	0.4 g/L

3.2 Rolling fatigue life under clean lubrication conditions

After operation for 10,000 h or more in all cases, the ETFA bearings were stopped in undamaged condition. Therefore, life under clean lubrication conditions was clearly longer than the basic rating life under these test conditions (L_{10h} = 243 h).

3.3 Rolling fatigue life under contaminated lubrication conditions

Fig. 7 shows results of the test under contaminated lubrication conditions. Rolling fatigue life of the ETFA bearing under contaminated lubrication conditions is roughly 2 times or more greater than that of the conventional product.

Flaking due to rolling fatigue can be broadly divided into two types depending on differences in the point of damage origin: surface originated and subsurface originated[11)-13)]. In both cases, the magnitude of stress concentration due to rolling has an effect on life. Therefore, it is conjectured that ETFA has some effectiveness in easing stress concentration during rolling.

In flaking under contaminated lubrication conditions, the damage originates at the margin of an indentation formed by a hard foreign body. This sort of indentation-originated flaking is thought to occur due to application of repeated normal stress at the surface normal to the raceway tangent direction[14)]. The fatigue strength of low-carbon steel after carburizing improves with greater refinement of prior γ grain[15)]. Therefore, rolling fatigue life of the developed product under contaminated lubrication conditions is thought to improve due to block refinement.

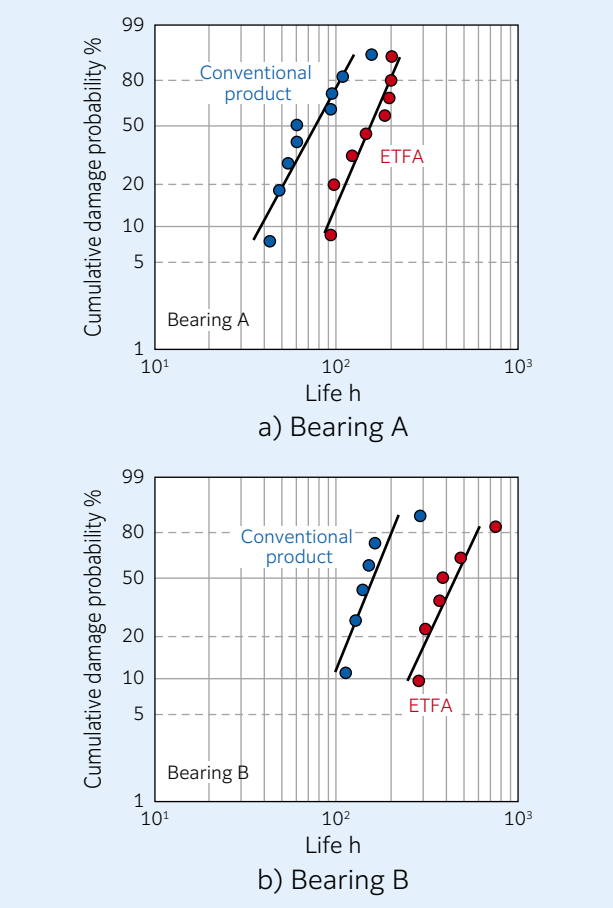

Fig. 7 Results of the life tests under contaminated lubrication conditions

4. ETFA impact strength

4.1 Impact test conditions

A Charpy impact test was carried out at room temperature and low temperature (-20 ℃). The test specimen was the U-notch type with dimensions of 55 mm × 10 mm × 10 mm. The test method conformed to JIS Z 2242.

4.2 Impact strength

Table 3 shows the results of the Charpy impact test. Impact strength of ETFA was roughly 1.8 times that of conventional material.

Table 3 Charpy impact values of the specimens at room temperature and – 20 ℃

[J/cm^2]

Test material / Test temperature	Conventional material	ETFA
Room temperature	5.3	9.8
Low temperature (-20 ℃)	5.0	9.5

4.3 Reason for improving toughness

Fig. 8 shows observation images of the fracture surface near the notch bottom of the impact test specimen, and Cr mapping images of the fields of observation. A SEM was used for observation, and energy-dispersive X-ray spectroscopy (EDX) was used for Cr mapping. Enlargements of the observed fields a) and d) are given in b) and e). Mapping images were obtained for observed fields b) and e). In addition, the region of ductile crack formation prior to fracture is indicated with a dotted line in the images for observed fields a) and d)[16)].

The main fracture morphology of the conventional material was grain boundary fracture at prior γ grain boundaries. The width of the ductile crack formation region was about 5 μm. Also, dispersion of Cr-based precipitations was confirmed at the prior γ grain boundary surface, and the size of the precipitations was roughly 500 nm or less.

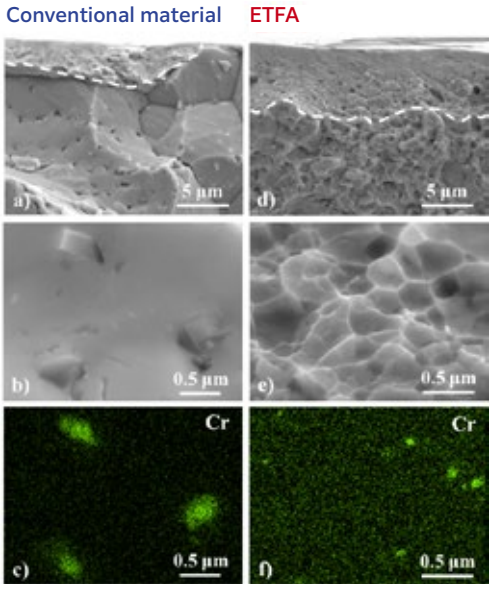

Fig. 8 SEM-micrographs and EDX-mappings of the fracture surfaces near the U-notch after impact test

On the other hand, the main fracture morphology of ETFA was transgranular fracture. Width of the ductile crack formation region was about 10 μm. Numerous dimples were confirmed at the fracture surface, and their size was roughly 50 – 500 nm. Dispersion of Cr-based precipitations was also confirmed at the fracture surface. Their size was roughly 100 nm or less.

For the above reasons, it is thought that grain boundary segregation of precipitations containing Cr is suppressed in ETFA, and prior γ grain boundaries are strengthened[17]. Also, the region where ductile cracking forms expands, and thus it is likely that fracture stress has been increased due to transgranular plastic deformation[18)-20)]. Improved toughness likely occurred due to refinement of blocks and precipitation structure.

5.ETFA wear resistance

5.1 Wear test conditions

A Savin type wear test was conducted at room temperature[21)]. **Fig. 9** shows a schematic drawing of the test rig, and **Table 4** gives the test conditions. The test specimen was sheet-shaped with dimensions 15 mm × 6 mm × 3 mm. The rotating circular plate serving as the opposing material has an outer diameter of 40 mm, and a subcurvature of R 60.

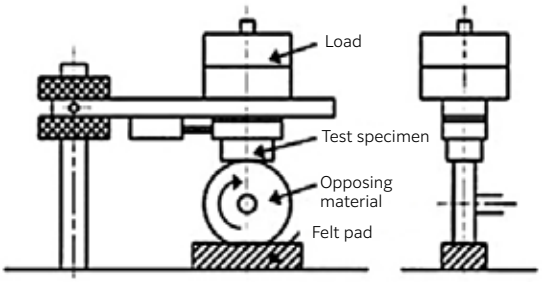

Fig. 9 Schematic drawing of Savin type wear test rig

Table 4 Condition of the wear test

Item	Setting conditions
Load	50 N
Initial max. contact surface pressure	0.49 GPa
Sliding speed	0.05 m/s
Sliding time	60 min
Lubricating oil viscosity grade	ISO VG 2
Lubrication type	Felt pad lubrication
Opposing material diameter	40 mm
Opposing material sub-curvature	R 60
Opposing material surface roughness	Ra 0.01 μm

5.2 Wear resistance

Table 5 shows the specific wear rate obtained from the wear test. The specific wear rate of ETFA was compared with that of the conventional material, and it was about 1/2 or less. Based on the order of the specific wear rate, it is conjectured that the main wear mode is adhesive wear [22)].

Table 5 Specific wear rate of the specimens

[× 10^{-10} $mm^3/(N \cdot m)$]

Test material / Opposing material	Conventional material	ETFA
Conventional material	701	120
ETFA	357	166

5.3 Reason for improved wear resistance

Fig. 10 shows optical microscope images, SEM images, and oxygen mapping images obtained through EDX, of the test specimen wear traces. The wear traces of the conventional material form a number of streaks due to wear scratching in the sliding direction (vertical direction). ETFA, on the other hand, exhibits wear scratches with a fine line width over a wide range. Oxidation was evident in the region where these wear scratches occurred.

Compared with conventional material, ETFA has high toughness, and hard, fine precipitations are dispersed homogeneously over the surface, and those precipitations and high toughness are thought to raise the shear resistance of the direct contact surface. As a result, it is likely that severe wear was suppressed, and high surface pressure was maintained at the contact surface, so that oxidation at the wear surface was promoted [23)24)].

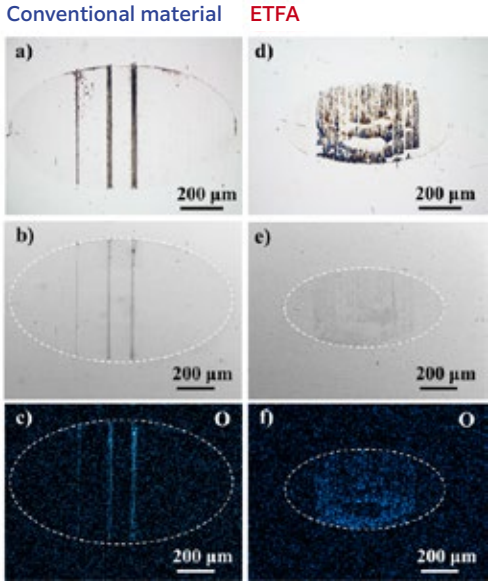

Fig. 10 Optical micrographs, SEM-micrographs and oxygen mappings of the wear traces for the specimens

6. Conclusion

This article has described in detail "ETFA" roller bearings strengthened through fine microstructure design. The rolling fatigue life and strength characteristics of these bearings greatly surpass conventional bearings, and thus ETFA can cope with the increasing severity of roller bearing use environments.

We at **NTN** will continue improving our heat treatment and material technologies, and contributing to the development of roller bearings.

References

1) R. A. Grange, ASM Trans Quart., 59, (1966) 26.
2) G. Krauss, Deformation and Fracture in Martensitic Carbon Steels Tempered at Low Temperatures, Metallurgical and Materials Transactions A, (2001) 861.
3) Tadashi Maki, Imao Tamura, Morphology and Substructure of Lath Martensite in Steels, Tetsu-to-Hagane (Iron and Steel), 67, (1981) 852.
4) Yuuji Kimura, Kaneaki Tsuzaki, Trends in Technology for Refinement of Martensite Structure, The Special Steel, 52, (2003) 12.
5) S. Morito, H. Yoshida, T. Maki and X. Huang, Effect of Block Size on the Strength of Lath Martensite in Low Carbon Steels, Materials Science and Engineering A, 438-440, (2006) 237.
6) Akinobu Shibata, Martensite in Iron-based Alloy —the Formation Mechanism of Microstructure and the Origin of Mechanical Property —, Materia Japan, Bulletin of the Japan Institute of Metals, 50, (2011) 254.
7) Chikara Ohki, Improving Rolling Contact Fatigue Life of Bearing Steels Through Grain Refinement, SAE Tech. Paper Series, (2004) 01-0634.
8) Nobuyuki Mouri, Improvement of Carburized Steel Wear Resistance by Heat Treatment, Tribology Conference Proceedings, 2008, Fall, Nagoya.
9) Nobuyuki Mouri, Kazuhiko Taguchi, Improvement of Carburized Steel Wear Resistance by Heat Treatment, NTN TECHNICAL REVIEW, No. 76, (2008) 17.
10) Kikuo Maeda, Hirokazu Nakashima, Hiroshi Kashimura, Development of Long Life TAB and ETA Bearings and Their Automotive Applications, NTN TECHNICAL REVIEW, No. 65, (1996) 17.
11) W. E. Littmann and R. L. Winder, Propagation of Contact Fatigue from Surface and Subsurface Origins, Transactions of ASME, D, 88, (1966) 624.
12) T. E. Tallian and J. I. McCool, An Engineering Model of Spalling Fatigue Failure in Rolling Contact, Wear, 17, (1971) 447.
13) Y. P. Chiu, T. E. Tallian and J. I. McCool, An Engineering Model of Spalling Fatigue Failure in Rolling Contact, Wear, 17, (1971) 433.
14) Toru Ueda, Takashi Sakaguchi, Naoya Seno, Shigeru Okita, Nobuaki Mitamura, Flaking Morphology in a Contaminated Lubrication Environment — Effects of Tangential Force on Indentation-Originated Flaking —, NSK Technical Journal, 685, (2012) 58.
15) C. A. Apple and G. Krauss, Microcracking and Fatigue in a Carburized Steel, Metallurgical Transactions, 4, (1973) 1195.
16) Toshiro Kobayashi, Evaluation of Impact Fracture Characteristics of Metal Materials at Low Temperatures using the Instrumented Charpy Test Method, Bulletin of the Japan Institute of Metals, (1973) 546.
17) Riichi Murakami, Yunhe Kim, Kazuhiro Kusukawa, Fundamentals of Material Strength and Fracture, Nishinihonhouki Shuppan, (2005) 62.
18) Seiichi Karashima, Metal and Alloy Strength, Japan Institute of Metals and Materials, (1972) 134.
19) Toshiro Kobayashi, Koichi Takai, Evaluation of Mechanical Fracture Behavior of Metal Materials at Low Temperature, Fuji Electric Journal, 46, (1973) 235.
20) T. Hanamura, F. Yin and K. Nagai, Ductile-Brittle Transition Temperature of Ultrafine Ferrite/Cementite Microstructure in a Low Carbon Steel Controlled by Effective Grain Size, ISIJ International, 44, (2004) 610.
21) Makio Mizuno, Measurement of Abrasion Loss, Journal of Japan Society of Lubrication Engineers, 25, (1980) 801.
22) Mechanical Engineers Handbook B1, Japan Society of Mechanical Engineers, (1985) 61.
23) Tadashi Sasada, Wear, Yokendo, (2008) 48.
24) Yuji Yamamoto, Motohiro Kaneta, Tribology 2nd Edition, Ohmsha, (2010) 195.

Photo of authors

Masahiro YAMADA
Advanced Technology R&D Center

Naota YAMAMOTO
Application Engineering Dept., Industrial Business Headquarters

Chikara OHKI
Advanced Technology R&D Center